



1 **Reconstructing seasonality through stable isotope and trace element analysis of the Proserpine**  
2 **stalagmite, Han-sur-Lesse Cave, Belgium: indications for climate-driven changes during the last 400**  
3 **years**

4 Stef Vansteenberge<sup>1\*</sup>, Niels de Winter<sup>1</sup>, Matthias Sinnesael<sup>1</sup>, Sophie Verheyden<sup>2,1</sup>, Steven Goderis<sup>1,3</sup>,  
5 Stijn J. M. Van Malderen<sup>3</sup>, Frank Vanhaecke<sup>3</sup> and Philippe Claeys<sup>1</sup>.

6 <sup>1</sup>Department of Analytical, Environmental and Geochemistry, Vrije Universiteit Brussel, Pleinlaan 2, B-  
7 1050 Brussels, Belgium.

8 <sup>2</sup>Royal Belgian Institute of Natural Sciences, Jennerstraat 13, B- 1000 Brussels, Belgium

9 <sup>3</sup>Department of Analytical Chemistry, Ghent University, Campus Sterre, Krijgslaan 281 S12, B-9000  
10 Ghent, Belgium

11 **\*Corresponding author: Niels.de.winter@vub.be**

12

13



## 14 Abstract

15 Annually laminated speleothems allow the reconstruction of paleoclimate down to a seasonal scale. In  
16 this study, an annually laminated stalagmite from the Han-sur-Lesse Cave (Belgium) is used to study  
17 the expression of the seasonal cycle in northwestern Europe during the Little Ice Age. More specifically,  
18 two historical 12-year-long growth periods (ca. 1593-1605 CE and 1635-1646 CE) and one modern  
19 growth period (1960-2010 CE) are analysed on a sub-annual scale for their stable isotope ratios ( $\delta^{13}\text{C}$   
20 and  $\delta^{18}\text{O}$ ) and trace element (Mg, Sr, Ba, Zn, Y, Pb, U) content. Seasonal variability in the proxies is  
21 confirmed with frequency analysis. Zn, Y and Pb show distinct annual peaks in all three investigated  
22 periods related to annual flushing of the soil during winter. A strong seasonal in phase relationship  
23 between Mg, Sr and Ba in the modern growth period reflects a substantial influence of prior calcite  
24 precipitation (PCP). In particular, PCP occurs during summers when recharge of the epikarst is low. This  
25 is also evidenced by earlier observations of increased  $\delta^{13}\text{C}$  values during summer. In the 17<sup>th</sup> century  
26 intervals, there is a distinct antiphase relationship between Mg, Sr and Ba, suggesting that varying  
27 degrees of incongruent dissolution of dolomite control the observed seasonal variations. The  
28 processes controlling seasonal variations in Mg, Sr and Ba in the speleothem appear to change  
29 between the 17<sup>th</sup> century and 1960-2010 CE. The Zn, Y, Pb and U concentration profiles, stable isotope  
30 ratios and morphology of the speleothem laminae all point towards increased seasonal amplitude in  
31 cave hydrology and higher drip water discharge during the 17<sup>th</sup> century. These observations reflect an  
32 increase in water excess above the cave and recharge of the epikarst, due to a combination of lower  
33 summer temperatures and increased winter precipitation during the 17<sup>th</sup> century. This study indicates  
34 that the transfer function controlling Mg, Sr and Ba seasonal variability varies over time. Which process  
35 is dominant, either PCP or dolomite dissolution, is clearly climate-driven and can thus be used as a  
36 paleoclimate proxy itself.

37 **Keywords:** Speleothem, seasonality, Little Ice Age, trace element concentrations, stable isotope ratios,  
38 proxy transfer functions

## 39 1. Introduction

40 Speleothems have been successfully used to reconstruct paleoclimate on various time scales (Fairchild  
41 and Baker, 2012), from tropical latitudes (e.g. Wang et al., 2001) to temperate areas (e.g. (Genty et al.,  
42 2003). Their ability to hold distinct annual layering enables paleoclimate reconstructions down to  
43 seasonal scale. The occurrence of visible annual laminae in speleothems has been reported from sites  
44 all over the world (Baker et al., 2008). A common expression of this visible layering is an alternation of  
45 dark compact laminae (DCL) and white porous laminae (WPL), as defined by Genty and Quinif (1996).  
46 According to Baker et al. (2008), the origin of visible seasonal layering is related to seasonal variations



47 in drip rate, in drip water supersaturation and/or in cave climatology. However, in most cases, visible  
48 seasonal layering is formed by changes in drip water discharge (Baker et al., 2008). Such changes in  
49 drip rate often coincide with the presence of a varying degree of prior calcite precipitation (PCP). PCP  
50 is the process of calcite precipitation upstream of the site of speleothem deposition (Fairchild et al.,  
51 2000). An increase in PCP occurs when the ability of cave waters to degas increases. Therefore, a higher  
52 degree of PCP is attributed to drier periods (Fairchild et al., 2000; Fairchild and Treble, 2009). Variations  
53 in the amount of PCP have been observed on a seasonal scale (e.g. Johnson et al., 2006). The presence  
54 of seasonally laminated speleothems in Belgian cave systems is known for several decades (e.g. Genty  
55 and Quinif, 1996). The best known example is the Proserpine stalagmite collected from Han-sur-Lesse  
56 Cave and first described by Verheyden et al. (2006). The speleothem has a well-expressed visual and  
57 geochemical seasonal layering over the last 500 years according to layer counting and U/Th dating (Van  
58 Rampelbergh et al., 2014). This geochemical layering is reflected by sub-annual variations of stable  
59 isotope ratios ( $\delta^{13}\text{C}$  and  $\delta^{18}\text{O}$ ). A thorough understanding of modern seasonal control on variations in  
60  $\delta^{13}\text{C}$  and  $\delta^{18}\text{O}$  in speleothem calcium carbonate results from rigorous monitoring of the conditions at  
61 the sample site in Han-sur-Lesse cave as carried out by Van Rampelbergh et al. (2014) for the period  
62 2012-2014.

63 In addition to the commonly used speleothem  $\delta^{18}\text{O}$  and  $\delta^{13}\text{C}$  proxies, the use of trace elemental  
64 concentrations (e.g. Mg, Sr, Ba, Zn and U) as paleoclimate and paleoenvironmental proxies is becoming  
65 standard practice in speleothem reconstructions (Fairchild et al., 2000; Regattieri et al., 2016). The use  
66 of trace elements brings additional information that can be used to unravel seasonal variability in  
67 speleothem chemistry. Examples of this include the use of trace element concentrations as proxies for  
68 precipitation (Baldini et al., 2002; Warken et al., 2018), soil processes (Regattieri et al., 2016) or  
69 changes in sediment supply (Regattieri et al., 2016) and can be used to identify volcanic ash fall events  
70 from speleothem records (Jamieson et al., 2015).

71 The first objective of this study is to better characterize the geochemical layering by adding trace  
72 element proxies to improve the understanding of processes driving the geochemical layering and to  
73 further resolve the relation with seasonal climatic variability. In addition, this work also compares the  
74 seasonal cycle within earlier identified cold periods (Verheyden et al., 2006; Van Rampelbergh et al.,  
75 2015; Supp. Mat. Fig. 1) to present-day seasonal signals. To achieve this, two 12-year long stalagmite  
76 growth periods (1593-1605 CE  $\pm$  30, hereafter P16 and 1635-1646 CE  $\pm$  30, hereafter P17) and a recent  
77 analogue deposited between 1960-2010 CE (hereafter referred to as P19) are analysed on a sub-annual  
78 scale for their stable isotopic ( $\delta^{13}\text{C}$  and  $\delta^{18}\text{O}$ ) and trace elemental variations. This information is then  
79 interpreted in terms of climatic changes during the last 400 years.



80 **2. Geological setting**

81 **2.1 Han-sur-Lesse Cave**

82 With a total length of approximately 10 km, the Han-sur-Lesse Cave system, located within a limestone  
83 belt of Middle Devonian age, is the largest known subterranean karst network in Belgium (Fig. 1A). The  
84 cave system was formed by a meander cut-off of the Lesse River within the Massif de Boine, which is  
85 part of an anticline structure consisting of Middle to Late Givetian reefal limestones (i.e. the Mont-  
86 d'Hours and Fromelennes Formations (Fm.); Delvaux de Fenffe, 1985). The thickness of the epikarst  
87 zone above the cave is estimated to be around 40 m (Quinif, 1988). Studies have shown the local  
88 presence of dolomite in these Givetian limestones. Within the Mont-d'Hours Fm., the biostromal  
89 limestones are alternated with fine-grained micritic limestones and dolomitic shales (Preat and  
90 Bultynck, 2006). Additionally, a recent study by Pas et al. (2016) on Middle Devonian outcrops has  
91 shown that dolomitized beds also occur within the limestones of the Fromelennes Fm.

92 The Han-sur-Lesse Cave is located ~200 km inland at an elevation of 200 m above sea level. The region  
93 is marked by a warm temperate, fully humid climate with cool summers, following the Köppen-Geiger  
94 classification (Kottek et al., 2006). In the period 1999-2013, annual temperatures averaged 10.2 °C and  
95 average annual rainfall amount was 820 mm yr<sup>-1</sup> in Rochefort, 10 km from Han-sur-Lesse (Royal  
96 Meteorological Institute). The study site is affected by a North Atlantic moisture source all year round  
97 (Gimeno et al., 2010) and the amount of precipitation does not follow a seasonal distribution.  
98 Calculations applying the Thornthwaite formula (Thornthwaite and Mater, 1957) show that there is a  
99 strong seasonal trend in the water excess, i.e. the amount of rainfall minus the amount lost by  
100 evapotranspiration, with water excess only occurring from October to April (Genty and Deflandre,  
101 1998; Genty and Quinif, 1996).

102 The studied speleothem was retrieved from the Salle-du-Dôme, a 150 m wide and 60 m high chamber  
103 that formed by roof-collapse of the limestone (Fig 1B). The Salle-du-Dôme is well ventilated, as it is  
104 located close to the cave exit and connected through two passages to nearby chambers. Monitoring  
105 of cave atmosphere within the Salle-du-Dôme for the period 2012-2014 showed that in 2013 the  
106 temperature inside the chamber varied seasonally between 10.5 and 14.5 °C (Van Rampelbergh et al.,  
107 2014). Similar seasonal trends in temperature are observed for the drip water, but the average is 0.5  
108 °C colder. The pCO<sub>2</sub> of the cave air averages around 500 ppmv for the whole year. Yet, in summer (July-  
109 August), a rapid and temporary increase to 1000 ppmv is observed. Also during summer, rainwater  
110 δ<sup>18</sup>O and δD above the cave increase by 3 ‰ and 30 ‰ (VSMOW, Vienna Standard Mean Ocean Water)  
111 respectively, likely due to the atmospheric temperature effect as described by Rozanski et al. (1992).  
112 In contrast, drip water δ<sup>18</sup>O and δD remain fairly stable throughout the year, with averages of -7.65 ‰



113 and -50.1 ‰ VSMOW and standard deviations of 0.07 ‰ and 0.6 ‰ VSMOW, respectively. During late  
114 summer (September), an increase of 1.5 ‰ is observed in the  $\delta^{13}\text{C}$  record of dissolved inorganic carbon  
115 (DIC) within the drip water

## 116 **2.2 Proserpine speleothem**

117 The Proserpine speleothem is a 2 m high, tabular shaped stalagmite. The speleothem has a surface  
118 area of 1.77 m<sup>2</sup> and is fed by a drip flow with drip rates ranging between 100 and 300 mL min<sup>-1</sup>. The  
119 speleothem grew over a period of approximately 2 kyr and has thus an exceptionally high average  
120 growth rate of 1 mm yr<sup>-1</sup>. The large speleothem was drilled and a 2 m long core was retrieved. The  
121 upper 50 cm of this core, dating back to approximately 1500 CE (Supp. Mat. Fig. 2), shows a well-  
122 expressed layering of alternating DCL and WPL (Verheyden et al., 2006). Previous studies concluded  
123 that multi-decadal simultaneous changes in different proxies (such as crystal fabric, growth rate, layer  
124 thickness, and oxygen and carbon stable isotope ratios) indicate that these are controlled by common  
125 climatic, environmental or anthropogenic factors, despite the observation that some parts of the  
126 Proserpine speleothem appear to have been deposited out of isotopic equilibrium with the drip water  
127 (Verheyden et al., 2006; Van Rampelbergh et al., 2015). Based on a detailed cave monitoring study at  
128 the Proserpine site in the years 2012 to 2014, Van Rampelbergh et al. (2014) showed that  $\delta^{18}\text{O}$  and  
129  $\delta^{13}\text{C}$  of seasonally deposited calcite reflect isotopic equilibrium conditions and that variations of stable  
130 isotope ratios are induced by seasonal changes. These seasonal changes in stable isotope ratios  
131 correspond with the observed visible layering. The speleothem  $\delta^{18}\text{O}$  value is believed to reflect changes  
132 in seasonal cave climatology. While drip water  $\delta^{18}\text{O}$  remains constant, calcite  $\delta^{18}\text{O}$  decreases with ~0.6  
133 ‰ in summer months, caused by temperature-dependent fractionation during calcite precipitation.  
134 This fractionation was calculated to be -0.2 ‰ °C<sup>-1</sup>. In contrast,  $\delta^{13}\text{C}$  reflects seasonal changes occurring  
135 at the epikarst level. A ~1.5 ‰ increase of  $\delta^{13}\text{C}$  in drip water DIC during late summer is directly reflected  
136 in the freshly deposited speleothem calcite. The enrichment in drip water  $\delta^{13}\text{C}$  values occurs shortly  
137 after the observed decrease in drip water discharge, and therefore seasonal variations in the degree  
138 of prior calcite precipitation in the epikarst has been hypothesized to be the main driver of seasonal  
139  $\delta^{13}\text{C}$  changes in the drip water (Van Rampelbergh et al., 2014).

## 140 **2.3 Dating**

141 The age-depth model of the Proserpine speleothem core has been established and discussed by Van  
142 Rampelbergh et al. (2015) and is provided in the supplementary material (Supp. Mat. Fig. 2). This age-  
143 depth model was constructed by using a combined approach of U-Th radiometric dating, based on 20  
144 U-Th ages, and layer counting. This has shown that the amount of counted layers is in good agreement  
145 with the U-Th ages (see Table 2 in Van Rampelbergh et al., 2015). However, at 9 to 10 cm from the top



146 of the core, a perturbation with heavily disturbed calcite occurs, making it impossible to construct a  
147 continuous layer counted chronology. Remains of straw and soot were found within this perturbation,  
148 suggesting that at that time, fires were lit on the speleothem's paleosurface (Verheyden et al., 2006).  
149 Layer counting gave an age of  $1857 \pm 6$  CE for the reestablishment of calcite deposition after the  
150 perturbation and U-Th age-depth modeling showed that the start of the perturbation occurred at  $1810$   
151  $\pm 45$  CE (Van Rampelbergh et al., 2015). Radiocarbon dating of the straw fragments embedded in the  
152 calcite gave an age between 1760 and 1810 CE, with 95.4 % probability. The age of  $1810 \pm 45$  CE is  
153 used to restart the layer counting after the perturbation towards the bottom of the core. This gave an  
154 age of 1593 to  $1605 \pm 30$  CE for P16 and  $1635$  to  $1646 \pm 30$  CE for P17. The more recent section P19  
155 studied here is situated above the perturbation and its age could be confidently established through  
156 annual layer counting at 1960-2010 CE.

157

### 158 3. Methods

#### 159 3.1 Analytical procedures

160 The three growth periods studied are shown in Fig. 2 and their age is derived from an age-depth model  
161 based on U-Th-dating and layer counting (Verheyden et al., 2006; Van Rampelbergh et al., 2015). For  
162  $\delta^{13}\text{C}$  and  $\delta^{18}\text{O}$  analysis, powder samples are acquired using a Merchantek Micromill  
163 (Merchantek/Electro Scientific Industries Inc. (ESI), Portland (OR), USA, coupled to Leica GZ6, Leica  
164 Microsystems GmbH, Wetzlar, Germany) equipped with tungsten carbide dental drills with a drill bit  
165 diameter of 300  $\mu\text{m}$ . The powders are stored in a 50 °C oven prior the analysis to avoid  $\delta^{13}\text{C}$  and  $\delta^{18}\text{O}$   
166 isotopic contamination. Measurements for P16 and P17 are carried out on a Nu Perspective isotope  
167 ratio mass spectrometer (IRMS) coupled to a Nucarb automated carbonate preparation device (Nu  
168 Instruments, UK) at the Vrije Universiteit Brussel (Belgium). The  $\delta^{13}\text{C}$  and  $\delta^{18}\text{O}$  records of P16 and P17  
169 consist of 201 and 116 data points, respectively, resulting in temporal resolutions of  $\sim 20$  and  $\sim 10$  data  
170 points per year, respectively. The analysis of the P19 interval is an extension of the previously published  
171 seasonally resolved 1976-1985 transect (Van Rampelbergh et al., 2014) and is carried out on a Delta  
172 plus XL IRMS coupled to a Kiel III carbonate preparation unit (Thermo Fisher Scientific, Germany) also  
173 at the Vrije Universiteit Brussel. For P19, a total of 350 samples are analysed, providing a temporal  
174 resolution of  $\sim 7$  data points per year. Within each batch of ten samples, the in-house reference  
175 material MAR2-2, prepared from Marbella limestone and calibrated against NBS-19 (Friedman et al.,  
176 1982) is measured together with the samples to correct for instrumental drift ( $\delta^{13}\text{C}$ :  $3.41 \pm 0.10$  ‰ (2s)  
177 VPDB;  $\delta^{18}\text{O}$ :  $0.13 \pm 0.20$  ‰ (2s) VPDB). All results are displayed as ‰VPDB (Vienna Pee Dee Belemnite)  
178 with the individual reproducibility reported as 2 standard deviation (SD) uncertainties. Averages of the



179 total 2 SD uncertainties for  $\delta^{13}\text{C}$  and  $\delta^{18}\text{O}$  are 0.03 ‰ and 0.09 ‰ for the Nu Perspective setup. With  
180 the Delta plus XL setup these are slightly higher, being 0.04 ‰ and 0.10 ‰ for  $\delta^{13}\text{C}$  and  $\delta^{18}\text{O}$ ,  
181 respectively (Van Rampelbergh et al., 2014).

182 Trace element variations are determined using inductively coupled plasma-mass spectrometry  
183 complemented by a laser ablation sample introduction system (LA-ICP-MS) at Ghent University  
184 (Belgium). The LA-ICP-MS setup consists of a 193 nm ArF\*excimer Analyte G2 laser ablation system  
185 (Teledyne Photon Machines, Bozeman, MT, USA) coupled to a single-collector sector field 'Element XR'  
186 ICP-MS unit (Thermo Fisher Scientific, Bremen, Germany). The laser is used to sample adjacent  
187 positions along a line segment parallel to the stalagmite's growth axis. The positions are ablated one-  
188 by-one for 15 s with a laser spot size of 50  $\mu\text{m}$  in diameter, a repetition rate of 30 Hz and a beam energy  
189 density of 3.51  $\text{J cm}^{-2}$ . The line segments for P16, P17 and P19 are drilled at 287, 249 and 445 individual  
190 positions, respectively. Sampling via individual drilling points is preferred over the conventional  
191 approach of continuous line scanning because the single positions can be sampled longer, resulting in  
192 an improved limit of detection. To carry out the analyses, the speleothem sections and reference  
193 materials are mounted in a HELEX 2 double-volume ablation cell. The Helium carrier gas ( $0.5 \text{ L min}^{-1}$ ) is  
194 mixed with Argon make-up gas ( $0.9 \text{ L min}^{-1}$ ) downstream of the ablation cell, and introduced into the  
195 ICP-MS unit, operated in low mass-resolution mode. Transient signals for Magnesium (Mg), Aluminium  
196 (Al), Silicon (Si), Phosphorus (P), Sulphur (S), Potassium (K), Iron (Fe), Manganese (Mn), Zinc (Zn),  
197 Rubidium (Rb), Strontium (Sr), Yttrium (Y), Barium (Ba), Lead (Pb), Thorium (Th), and Uranium (U) are  
198 monitored during analysis of the laser-induced aerosol. Cool plasma conditions (800 W RF power) are  
199 used to reduce Argon-based interferences and to increase the sensitivity of the analysis. A gas blank  
200 subtraction is performed on the data acquired at each position, based on the signal acquired 10 s prior  
201 to the ablation. Precise and accurate trace element concentration data are obtained from offline  
202 calibration, using seven international natural and synthetic glass and carbonate reference materials  
203 BHVO-2G, BIR-1G, GSD-1G, GSE-1G, and MACS-3 (United States Geological Survey) as well as SRM 610  
204 and 612 (National Institute of Standards and Technology). Ca is used as an internal standard, following  
205 the assumption that the calcium carbonate in the speleothem is made up of 38 wt. % Ca. Based on the  
206 reference materials and settings described, the repeatability for the produced elemental  
207 concentration data is typically on the order of 5% relative standard deviation (RSD). Limits of detection  
208 (LODs) are given in Table 1.

### 209 **3.2 Data Processing**

210 Frequency analysis is applied to study the variations in the different proxy signals, and allows  
211 evaluating which of these proxies records the seasonal cycle. The ability of frequency analysis to assess



212 the potential of a proxy to record the seasonal cycle in speleothems and other incremental climate  
213 archives is already recognized by Smith et al. (2009) and de Winter et al. (2017). Furthermore, the  
214 method can identify multi-annual trends or variability at the sub-seasonal level. Frequency analysis is  
215 performed using Fast Fourier Transformations (FFT) of the isotopic and trace element data in the  
216 distance domain. The data are de-trended and padded with zeros. The power spectra are plotted as  
217 simple periodograms with frequencies plotted in the distance domain ( $\text{mm}^{-1}$ ) to allow intuitive  
218 interpretation. The significance level (95%) is evaluated using Monte Carlo noise simulations. The  
219 routine used operates in MATLAB® and is based on the scripts provided in Muller and MacDonald  
220 (2000), which are explained in more detail in Bice et al. (2012).

221

222 An effective method to compare sub-annual variations of different proxies with each other is by  
223 resampling multiple annual cycles at a regular interval and stacking the individual cycles (Treble et al.,  
224 2003; Johnson et al., 2006; Borsato et al., 2007; de Winter et al. 2018). The advantage of this method  
225 is that the phase-relations of the different proxies are preserved (Treble et al., 2003). Annual stacks  
226 are created based on the moving averages to diminish the influence of low-frequency noise on the  
227 annual stacks. The number of points used for moving averages is determined as a function of the  
228 sampling resolution (i.e., 3-point moving average for stable isotope records and 5-point moving  
229 average for trace element records, see Fig. 5). Proxy records with well-constrained seasonal variation  
230 are used to define seasonal cycles. In this study, individual years are selected based on  $\delta^{13}\text{C}$  (minima)  
231 for stable isotope records and Zn (maxima) for the trace element records. Stable isotope ratios and  
232 trace element stacks are created separately (Fig. 2). For P16 and P17, all annual cycles are included in  
233 the stack, except for the first and the last one, since there is no guarantee that these are entirely  
234 represented in the record. For P19, only ten years were selected from the full record to avoid any effect  
235 multi-decadal variability and to maintain an approach similar to that of P16 and P17. The years are  
236 indicated by the red line in Fig. 5.

#### 237 4. Results

238 The concentration range of each proxy measured in the three different intervals is shown in Fig. 3. For  
239  $\delta^{13}\text{C}$  and  $\delta^{18}\text{O}$ , the average values and ranges (minima to maxima) in P19 are significantly higher than  
240 those in P17 and P16. To illustrate the spread in the trace element records, the median is used instead  
241 of the average as it is less sensitive to large concentration ranges and outliers. Al, Si, K, Mn, Rb and Th  
242 are not included in this study since > 25% of the data falls below the LOD. An exception is made in the  
243 case of Y; few data points are retained for P17 (81% of the data is < LOD in P17 and 18% and 36% of  
244 the data is < LOD in P19 and P16 respectively. However, Y data are discussed because of the clear  
245 seasonal signal shown in P19 and P16 (Supp. Mat. Fig. 3 and 5).





246 Records of stable isotope ratios ( $\delta^{13}\text{C}$  and  $\delta^{18}\text{O}$ ) and trace element (Mg, Zn, Sr, Y, Ba, Pb and U)  
247 concentrations are plotted in the distance domain in Fig. 5. The occurrence of darker laminae (DCL) in  
248 the samples is indicated by blue bands, clearly showing that layers are thicker in P16 and P17 (average  
249 1.135 mm and 1.096 mm, respectively) compared to P19 (average 0.382 mm). For all intervals, the  
250 seasonal cycles are well constrained by  $\delta^{13}\text{C}$ , with lower  $\delta^{13}\text{C}$  values occurring in DCL. The average  $\delta^{13}\text{C}$   
251 is higher for P19 (-8.36 ‰) compared to P17 and P16 (-9.82 ‰ and -10.04 ‰, respectively). In addition,  
252 the amplitude of the individual cycles is larger in P19. Seasonal cycles in  $\delta^{18}\text{O}$  are much less  
253 pronounced. The most distinctive cycles are observed in P19 and some can be identified in parts of  
254 P17 and P16 (e.g. between 4 and 7 mm in P16 or between 3 and 7 mm in P17), while for other parts  
255 (e.g. between 7 and 11 mm in P16) they appear to be absent.

256 Seasonal variations are observed for Mg, Sr and Ba in all three intervals investigated (Fig 5). In P17 and  
257 P16, the median concentrations of these elements are closely related; 447 and 444  $\mu\text{g g}^{-1}$  for Mg, 51  
258 and 45  $\mu\text{g g}^{-1}$  for Sr and 36 and 33  $\mu\text{g g}^{-1}$  for Ba (Fig. 3). However, in P19 concentrations of Mg and Ba  
259 are slightly higher compared to the older intervals, i.e. 706  $\mu\text{g g}^{-1}$  for Mg and 46  $\mu\text{g g}^{-1}$  for Ba. This is  
260 also the case for Pb and U with concentrations significantly lower in P17 (0.14 and 0.05  $\mu\text{g g}^{-1}$ ,  
261 respectively) and P16 (0.14 and 0.07  $\mu\text{g g}^{-1}$ , respectively) and a seasonal cycle that is less pronounced  
262 than in P19 (0.37 and 0.18  $\mu\text{g g}^{-1}$ ). In contrast, P16 has the highest median concentrations of Zn (54  $\mu\text{g g}^{-1}$ )  
263 and Y (0.04  $\mu\text{g g}^{-1}$ ) and both elements display a well-defined seasonal covariation. Although the  
264 concentration of Zn is lower in P19 and P17 (14 and 25  $\mu\text{g g}^{-1}$ , respectively), the seasonal cycle is still  
265 present. Similar observations can be made for Y in P19 (0.02  $\mu\text{g g}^{-1}$ ). Within P16 and P17, maxima of  
266 Zn, Y, Sr and Ba mostly occur within the DCL.

267 Figure 4 shows an example of the FFT periodograms of  $\delta^{13}\text{C}$ , Mg, Zn and P in P16. Additional  
268 periodograms for the other elements in P16, P17 and P19 are included as supplementary data (Supp.  
269 Mat. Fig. 3-5). The frequency analysis confirms the clear seasonal cyclicity of  $\delta^{13}\text{C}$  previously observed  
270 by Van Rampelbergh et al. (2014) (Fig. 4). The dominant frequency of  $\delta^{13}\text{C}$  in P16 is 0.8  $\text{mm}^{-1}$  (Fig. 4).  
271 This corresponds to a period of 1.25 mm, which is in good agreement with an observed average layer  
272 thickness of 1.13 mm (Supp. Mat. Fig. 6). Because of its distinct seasonal cyclicity, the  $\delta^{13}\text{C}$  cycle is used  
273 as a reference to deduce whether or not other proxies record the seasonal cycle. Mg and Zn appear to  
274 track this seasonal cycle well as their periodograms contain peaks at 0.8 and 0.75  $\text{mm}^{-1}$  respectively,  
275 corresponding closely to the frequency of  $\delta^{13}\text{C}$ . For Zn, a broader double peak is observed with a main  
276 period of 1.18 mm and a smaller period of 1.02 mm. This double peak in the periodogram is caused by  
277 small variations in the thickness of the annual cycles around an average thickness of 1.14 m with a  
278 lightly skewed distribution towards thinner layers (see Supp. Mat. Fig. 6). The P record doesn't display



279 any significant seasonal cycle (95% confidence) (Fig. 4). For P19, visible layers are thinner (average  
280 0.382 mm) and also the variation in thickness is larger (RSD 28.9%) compared to P16 and P17 (Supp.  
281 Mat. Fig. 6). This results in broader and less well defined seasonal peaks in the periodograms.

## 282 5. Discussion

### 283 5.1 Seasonal cyclicity in trace element records

284 A schematic overview of the observed changes in the proxies discussed below and the interpretation  
285 for the three intervals is provided in Table 2. Assessing the exact phasing of the seasonal cycles of  
286 different trace elements to  $\delta^{13}\text{C}$  and the visible layering remains challenging since 1) often a multitude  
287 of factors control trace element variations within speleothems and 2) stable isotope ratios and the  
288 trace element concentrations are not measured on the same samples. An example of such a phase  
289 problem is the occurrence of an additional year in P16 in the trace element curve compared to  $\delta^{13}\text{C}$   
290 (Fig. 5, between 1 and 6 mm). Nevertheless, overall,  $\delta^{13}\text{C}$  minima occur in the DCL, suggesting a similar  
291 timing (and maybe control) on the visible laminae and  $\delta^{13}\text{C}$  cycles. Trace element proxies show cyclicity  
292 with a similar frequency as the  $\delta^{13}\text{C}$  (Fig. 4), in contrast to  $\delta^{18}\text{O}$  which seasonal cycles in P16 and P17  
293 are less clear.

#### 294 5.1.1 Zinc, yttrium and lead proxies

295 In earlier monitoring studies carried out in the Père-Noël Cave (also part of Han-sur-Less Cave system,  
296 Fig. 1), the presence of a late autumn increase in discharge was identified (Genty and Deflandre, 1998;  
297 Verheyden et al., 2008). In-situ conductivity measurements indicated an elevated mineral and/or  
298 organic matter increase during this autumnal increase in drip water discharge (Genty and Deflandre,  
299 1998; Verheyden et al., 2008). Measurements of the drip water discharge above the Proserpine  
300 stalagmite show that in late November, a doubling of the discharge volume occurs. This increased  
301 discharge is maintained until May, when a gradual decrease is observed (Van Rampelbergh et al.,  
302 2014). The timing of the elevated discharge agrees with the theoretical water excess occurring above  
303 the cave (Genty and Quinif, 1996). The observed seasonal cycle in Zn, Y and Pb in the intervals studied  
304 is likely caused by this annual winter flushing. Variations in these trace metal concentrations within  
305 annual speleothem layers have previously been attributed to the annual hydrological cycle. For  
306 instance, Borsato et al. (2007) linked the peak concentrations of F, P, Cu, Zn, Br, Y and Pb to the annual  
307 increase of soil infiltration during autumnal rainfall. Furthermore, it was suggested that the transport  
308 of such elements mainly occurs via natural organic matter (NOM) or other form of colloidal material.  
309 Enrichments of these soil-derived elements within speleothems are believed to be associated with high  
310 drip water flows (Fairchild and Treble, 2009). Studies have shown that trace metals, such as Cu, Ni, Zn,



311 Pb, Y and REE, are predominantly transported via complexing by NOM, of which the fraction size in the  
312 karstic waters ranges from nominally-dissolved to colloidal-to-particulate (Hartland et al., 2012; Wynn  
313 et al., 2014). In the case of Zn and Pb, Fairchild et al. (2010) have shown that in Obir Cave (Austria) the  
314 visible and ultra-violet lamination forms during autumn and is enriched in Zn, Pb and P. According to  
315 Wynn et al. (2014), the correspondence of distinct Zn and Pb peaks with the autumnal laminae is  
316 compelling evidence for a high-flux transport of these trace metals with NOM. However, in this study  
317 no distinct annual cycle within the P record is observed (Fig. 4). Phosphorus is considered soil derived  
318 as it originates from vegetation dieback (e.g. Baldini et al., 2002). Therefore, P has shown similar  
319 variations as observed in Zn, Y and Pb in previous studies (Borsato et al., 2007; Fairchild et al., 2010).  
320 In the Proserpine speleothem, no relation between P and other soil derived trace elements is detected.  
321 An explanation for this can be similar to that proposed by Frisia et al. (2012), being that P is not derived  
322 from soil leaching, but from other sources such as phosphate minerals present in the epikarst or  
323 microbiological activity.

324 Because of the distinct signature of the seasonal cycle in Zn, the Zn peaks are used as tie-points to  
325 create the annual stacks of other trace element records (Fig. 6), with lower concentrations occurring  
326 during periods of lower discharge and vice versa. The much higher Zn and Y peaks in P16 compared to  
327 P17 and P19 suggest an increased seasonality effect in discharge; therefore the accompanied annual  
328 flushing of the soil above cave appears more intense in the early 17<sup>th</sup> century. Concentrations of Pb  
329 are significantly higher in P19 compared to the other periods (median of 0.37  $\mu\text{g g}^{-1}$  versus 0.14  $\mu\text{g g}^{-1}$   
330 and 0.14  $\mu\text{g g}^{-1}$  in P16 and P17, respectively). An increase of Zn and Y in P19 similar to that in Pb is not  
331 observed, suggesting that the Pb-enrichment occurs at the soil level from another source. A study of  
332 Allan et al. (2015) on Pb isotope ratios in the in the same Proserpine stalagmite shows that the Pb  
333 concentrations are soil derived and originate from various sources of anthropogenic atmospheric  
334 pollution (coal, industrial activities, steel production and road dust). This explains well the observed  
335 higher Pb concentration in P19. Allan et al. (2015) identified increases in Pb concentration during 1945-  
336 1965 CE and 1975-1990 CE, which are in agreement with the observed higher Pb concentrations in this  
337 study between 20-18 mm and 13-5 mm. They also concluded that this 20<sup>th</sup> century anthropogenic  
338 pollution only affects Pb and none of the other elements used as paleoseasonality proxy in this study.

### 339 5.1.2 Magnesium, strontium and barium proxies

340 Figure 6 shows that the annual stacks of Sr and Ba exhibit correlate strongly within all three intervals,  
341 evidenced by Pearson correlation coefficients ( $r$ ) of 0.71, 0.97 and 0.82 for P19, P17 and P16,  
342 respectively with p-values much smaller than 0.01 (99% confidence level). Magnesium displays an  
343 antiphase relationship with Sr and Ba in P16 ( $r = -0.85$ , p-value =  $1.8 \cdot 10^{-7}$ ) whereas in P19 this



344 relationship is in phase ( $r = 0.64$ ,  $p\text{-value} = 7.2 \cdot 10^{-4}$ ). For P17, there is no significant relationship  
345 between Mg with Sr and Ba (low correlation,  $r = -0.13$ ,  $p\text{-value} = 0.53$ ). A strong covariation of Mg with  
346 Sr and Ba, as observed in P19, has previously been attributed to reflect the presence of prior calcite  
347 precipitation (PCP) in the epikarst above the cave, caused by the occurrence of drier periods (Fairchild  
348 et al., 2000), even on a seasonal scale (Johnson et al., 2006). The presence of PCP during late summer  
349 (with high evapotranspiration above the cave), when strongly reduced drip water discharge exists  
350 above the Proserpine stalagmite, has also been evoked to explain the enriched  $\delta^{13}\text{C}$  of freshly  
351 deposited calcite during the cave's summer mode (Van Rampelbergh et al., 2014). Despite the  
352 difficulties of accurately correlating trace elements and stable isotope proxies, there appears to be a  
353 good agreement between the P19 Mg and  $\delta^{13}\text{C}$  record, with maxima in Mg corresponding with maxima  
354 in  $\delta^{13}\text{C}$ , confirming the hypothesis of PCP control on these proxies. In contrast, the antiphase variation  
355 in Mg with respect to Sr and Ba observed in P16, suggests the involvement of other processes that  
356 dominate over PCP. A positive relationship between the Mg partition coefficient and temperature  
357 would be expected from thermodynamic considerations, and this has indeed been observed in  
358 experimental carbonate precipitation studies (Gascoyne, 1983; Rimstidt et al., 1998; Huang and  
359 Fairchild, 2001; Day and Henderson, 2013). In similar experiments, strontium partitioning into  
360 inorganic carbonate is known to remain constant with increasing temperatures but can be influenced  
361 by calcite precipitation rate (Day and Henderson, 2013). Faster precipitation of calcite causes an  
362 increased amount of lattice defects, resulting in an increased value for the partition coefficient of Sr  
363 (Pingitore and Eastman, 1986) and thus more Sr uptake in the calcite. Higher temperatures, combined  
364 with a decrease in drip water discharge, leading to decreased growth rates, could therefore  
365 theoretically explain the antiphase relationship of Mg and Sr. However, growth rates in P16 are rather  
366 high and additionally, it has been suggested that the variations of Sr and Mg in drip water chemistry  
367 are often significantly higher than those caused by the processes mentioned above. Roberts et al.  
368 (1998) concluded that the temperature-dependence of the Mg partition coefficient could theoretically  
369 explain the observed seasonal Mg variations, but not the multi-annual trends, for which hydrological  
370 changes are likely more important. Such observations have caused the interpretation of the Mg proxy  
371 to shift from a temperature relationship to an interpretation in terms of hydrological changes such as  
372 amount of water recharge in the epikarst (Fairchild and Treble, 2009). In this study, a more likely  
373 explanation for the P16 antiphase relation in Mg, Sr and Ba is the incongruent dissolution of dolomite  
374 ( $\text{CaMg}(\text{CO}_3)_2$ ; IDD), taking place during annual periods that are characterized by enhanced water-rock  
375 interaction. The presence of dolomite within lateral-equivalent Givetian limestone deposits in Belgium  
376 has been recognised by Pas et al. (2016). Dolomitized parts of the limestone host-rock were observed  
377 within the nearby Père-Noël Cave (Fairchild et al., 2001). During periods of decreased recharge, i.e.  
378 summer for the Han-sur-Lesse Cave, prolonged interaction between water and rock leads to saturation



379 of the karstic water with respect to  $\text{CaCO}_3$ . When saturation is reached, incongruent dissolution of  
380 dolomite (IDD) will start and  $\text{Ca}^{2+}$  concentration remains constant due to the precipitation of calcite  
381 (Lohmann, 1988). IDD increases the Mg/Ca of the drip water (Fairchild et al., 2000), but lowers the  
382 Sr/Ca and the Ba/Ca, because dolomite tends to have lower Sr and Ba contents with respect to calcite  
383 (Roberts et al., 1998). The IDD process is believed to overwhelm the PCP signal in P16 and is likely  
384 responsible for the observed antiphase relation. During winter recharge, saturation of the water in the  
385 epikarst with respect to calcite is not attained and dolomite does not dissolve.

386 The comparison of the annual stacks for Mg, Sr and Ba of the different intervals corroborates the idea  
387 that PCP is the main process controlling the seasonal variations of these trace elements in P19 based  
388 on the in-phase relation of Mg, Sr and Ba. Within P16, enhanced seasonality in recharge causes IDD to  
389 dominate over PCP. This explains the antiphase relation of Mg against Ba and Sr. Somewhere between  
390 the P16 and P19 periods, a turnover in the hydrological regime of the epikarst allowed PCP to become  
391 dominant over IDD in the seasonal variations in the proxies. Within P17, the relationship between Mg,  
392 Sr and Ba is less clear. This could point towards a change in hydrological regime between the periods  
393 of deposition of P16 and P19.

### 394 5.1.3 Uranium

395 In speleothems, U is thought to be mainly derived from bedrock dissolution (Bourdin et al., 2011;  
396 Jamieson et al., 2016) and to be subsequently transported by the ground water towards the  
397 speleothem (Fairchild and Baker, 2012). The partition coefficient of U is  $<1$  for calcite (Johnson et al.,  
398 2006; Jamieson et al., 2016). This causes U to be preferentially excluded from the calcite and enriched  
399 in the remaining drip water during the process of PCP. However, in P19, where PCP is evoked as the  
400 dominant process controlling Mg, Sr and Ba seasonal variations, an antiphase relationship of U with  
401 Mg, Sr and Ba is observed (Fig. 6). Johnson et al. (2006) concluded that scavenging of U as uranyl ion  
402 ( $\text{UO}_2^{2+}$ ) from the drip water onto the calcite crystal surfaces during PCP has a more dominant control  
403 on seasonal U variability than the partition coefficient. Such mechanism explains why U is antiphase  
404 with the Mg, Sr and Ba variations.

### 405 5.2 Seasonal variations in $\delta^{13}\text{C}$ and $\delta^{18}\text{O}$

406 To compare and understand the seasonal variations in  $\delta^{13}\text{C}$  and  $\delta^{18}\text{O}$ , annual stacks were created (Fig.  
407 7) by virtual resampling based on the occurrence of peaks in  $\delta^{13}\text{C}$  values as this proxy reflects the  
408 seasonal cycle best (Fig. 4). The minima in  $\delta^{13}\text{C}$  always occur in DCL, for P16 and P17. In P19, this  
409 relation is less clear, however on close inspection nearly all of the  $\delta^{13}\text{C}$  minima occur within the DCL  
410 (Fig. 5). Van Rampelbergh et al. (2014) suggested that seasonal changes in  $\delta^{13}\text{C}$  of recent calcite are



411 driven by changes in PCP. Higher  $\delta^{13}\text{C}$  values occur when more PCP is observed, i.e. during periods of  
412 lower recharge. The in phase variations of Mg, Sr and Ba in P19 described above supports the  
413 hypothesis of a seasonally changing degree of PCP. Seasonal variations in the amount of PCP and its  
414 effect on  $\delta^{13}\text{C}$  has previously been recognized in monsoon regions (Johnson et al., 2006; Ridley et al.,  
415 2015). During P16, seasonal changes in incongruent dolomite dissolution dominate the trace element  
416 variations of Mg versus Sr and Ba over PCP. However, since the main source of carbon in Han-sur-Lesse  
417 cave waters is the vegetation cover above the cave (Genty et al., 2001), IDD is not expected to change  
418 the  $\delta^{13}\text{C}$  signal. For example, a case study carried out by Oster et al. (2014) showed that an increase in  
419 IDD did not affect the  $\delta^{13}\text{C}$  of the speleothem significantly, despite a difference of  $\sim 0.5\text{‰}$  in  $\delta^{13}\text{C}$   
420 between the limestone and dolomite component in the host rock. Since  $\delta^{13}\text{C}$  is not affected by IDD,  
421 the influence of PCP on the  $\delta^{13}\text{C}$  remains observable. Indeed, similar as in P19, for both P17 and P16  
422  $\delta^{13}\text{C}$  minima occur within DCL, suggesting that these DCL layers were deposited by during seasonal  
423 periods of increased drip water discharge.

424 Observations from cave monitoring have shown that seasonal changes in cave temperature ( $11^\circ\text{C}$  -  
425  $15^\circ\text{C}$ ) are the main driver of  $\delta^{18}\text{O}$  variations in freshly deposited calcite ( $-7.0\text{‰}$  -  $-6.2\text{‰}$ ; Van  
426 Rampelbergh et al., 2014). The  $\delta^{18}\text{O}$  periodograms show that the seasonal cycle is less developed  
427 compared to  $\delta^{13}\text{C}$  (Fig. 4 and Supp. Mat. Fig. 3-5). This is also expressed in the annual stacks (Fig. 7).  
428 For P19, there is tendency towards a positive correlation of  $\delta^{13}\text{C}$  and  $\delta^{18}\text{O}$  but in P17 and P16 this is  
429 unclear. Although analysis of recent calcite have clearly shown that  $\delta^{18}\text{O}$  values are at least partly  
430 controlled by the cave temperature, interpretation of the seasonal  $\delta^{18}\text{O}$  changes is difficult due to the  
431 reduced seasonal cyclicality in the  $\delta^{18}\text{O}$  records compared to other proxies. However, average  $\delta^{18}\text{O}$   
432 values of speleothem calcite are obviously more depleted for P17 and P16 compared to P19 (Fig. 3 and  
433 Fig. 5). The hypothesis put forward here is that the lower average  $\delta^{18}\text{O}$  values of P16 point towards an  
434 increase in winter precipitation above the cave, since Van Rampelbergh et al. (2014) has shown that  
435 winter precipitation, such as the presence of snow, above Han-sur-Lesse cave causes a severe decrease  
436 in  $\delta^{18}\text{O}$  of the precipitation. Subsequently, this decrease is then transferred to the drip water and into  
437 the speleothem calcite.

### 438 **5.3 Variability in the seasonal cycle**

439 The observed changes of the seasonal variations in Mg, Sr and Ba between P19, P17 and P16 can only  
440 be explained by a change in the process controlling the seasonal variability in Mg, Sr and Ba. In the  
441 recent period, between 1960 and 2010 CE, PCP is identified as the main driver for seasonal changes in  
442 Mg, Sr, Ba trace element concentrations. This hypothesis is supported by the  $\delta^{13}\text{C}$  variations. In the  
443 17<sup>th</sup> century intervals, Mg, Sr and Ba variations suggest that incongruent dissolution of dolomite rather



444 than PCP, dominates the seasonal signal. Fairchild and Baker (2012) defined the term transfer function  
445 to describe the quantitative relation between the speleothem chemistry and changing cave  
446 environments or climate. In this case, there is a change in (qualitative) transfer function from  
447 incongruent dolomite dissolution to prior calcite precipitation. This change in transfer function is likely  
448 to be climate-controlled since there are no indications for drastic changes in cave morphology over the  
449 last 500 years, as interpreted from the long term stable isotope ratio record (Van Rampelbergh et al.,  
450 2015 and Supp. Mat. Fig. 1). It is known that the strength of the acting transfer function can be used  
451 as a paleoclimate proxy. For example, Jamieson et al. (2016) demonstrated that the seasonal (anti-  
452 )correlation between  $\delta^{13}\text{C}$  and U/Ca varies through time within a Common Era stalagmite from Belize.  
453 During drier years, reduced seasonal variability in prior aragonite precipitation causes U/Ca and  $\delta^{13}\text{C}$   
454 to correlate more positively compared to wetter years. This illustrates how a transfer function can be  
455 regarded as a valuable paleoclimate proxy. In any case, a certain threshold must be reached for a  
456 switch between transfer functions to take place. A prerequisite for PCP to occur is the presence of  
457 sufficient karstic voids filled with a gas phase characterized by a lower  $\text{pCO}_2$  than that with which the  
458 infiltrating waters previously equilibrated (Fairchild and Treble, 2009). The presence of such karstic  
459 voids is dependent on the multi-annual to decadal recharge amount of the karstic aquifer. Indeed, the  
460 average values of trace element concentrations imply an increased water availability during P16 and  
461 P17 compared to P19. More specifically peaks in soil-derived trace element concentrations (Zn and Y)  
462 are higher for P16, pointing towards enhanced flushing and an increased seasonality in water  
463 availability. An anthropogenic influence explains the higher concentrations of Pb in P19. In addition,  
464 trace element concentrations originating from host rock dissolution (Mg, Sr, Ba and U) are significantly  
465 lower for P16, resulting from lower multi-annual water residence time. Lastly, layers in P16 and P17  
466 are up to three times thicker compared to P19 (Fig. 2 and Supp. Mat. Fig. 6), which reflects higher  
467 growth rates. The positive relationship between water supply and growth rate has been demonstrated  
468 in the past (Baker et al., 1998; Genty and Quinif, 1996). In large and irregular shaped stalagmites, such  
469 as the Proserpine, within-layer thickness can often be quite large (Baker et al., 2008). The long-term  
470 layer thickness evolution shows a clear difference between the 17<sup>th</sup> century and present day. The  
471 significantly thinner layers during recent times clearly indicate that less water is available compared to  
472 the 17<sup>th</sup> century.

473 A straightforward explanation for the observed wetter cave conditions during, in particular, P16 is an  
474 increase in seasonal water excess. An elevated water excess can be caused by an increase in  
475 precipitation or a decrease in temperature. A lower temperature, especially during summer, results in  
476 a decreased evaporation of surface water. Calculations of present-day potential evapotranspiration  
477 (PET) with the Thornthwaite equation (Thornthwaite and Mather, 1957) for the period 1999-2012



478 show a negative water excess lasting from May to September (Fig. 8). Although the Thornthwaite and  
479 Mather (1957) method does not include vegetation effects, it is still a reliable tool to provide an idea  
480 of the effect of changes in the temperature and/or precipitation on the PET (Black, 2007). The effect  
481 of a temperature decrease during summer months on the water excess was simulated with an  
482 arbitrarily chosen 1°C temperature drop compared to the 1999-2012 average monthly temperature.  
483 Such a temperature drop appears to have only a minor influence (Fig. 8). A hypothetical increase of  
484 total annual rainfall with 200 mm, equally spread across 12 months, has a much larger effect on the  
485 water excess (Fig. 8). However, this would decrease the length of the annual interval during which no  
486 recharge occurs (i.e. only during June-July instead of May-September) providing less suitable  
487 conditions for dolomite dissolution to occur. Therefore, the most plausible explanation would be to  
488 have a stronger seasonal distribution in the amount precipitation (with more winter precipitation),  
489 whereas today no seasonality in the amount of rainfall is observed.

#### 490 **5.4 Implications for 17<sup>th</sup> century paleoclimate**

491 The majority of Common Era paleoclimate reconstructions are based on tree-ring data (D'Arrigo et al.,  
492 2006), although other records, for example historical documents (e.g., Dobrovlny et al., 2010), ice  
493 cores (e.g., Zennaro et al., 2014) or speleothems (e.g., Baker et al., 2011; Cui et al., 2012) are used as  
494 well. Over the last decades, consensus has been reached that changes in solar irradiance and volcanic  
495 activity are the main drivers of short-term natural climate variability during the last millennium (e.g.  
496 Crowley, 2000; Bauer et al., 2003). Interpretations of the stable isotope and trace element proxies  
497 obtained on the Proserpine speleothem show that a higher recharge state of the karstic aquifer  
498 characterizes the 17<sup>th</sup> century intervals compared to 1960-2010. Such an increase in recharge requires  
499 a decrease in evapotranspiration, which can result either from lower summer temperatures or higher  
500 total annual precipitation. Although it is difficult to discriminate between both, the effect of a total  
501 annual precipitation increase on the recharge is expected to be higher compared to a decrease in  
502 summer temperature (Fig. 8). Globally dispersed regional temperature reconstructions indicate that  
503 multi-decadal warm or cold intervals, such as the Medieval Warm Period or the Little Ice Age (LIA), are  
504 not global events. Yet, a global cooling trend starting at 1580 CE is observed in the majority of the  
505 reconstructions (PAGES 2k Consortium, 2013). Several paleoclimate reconstructions agreed upon the  
506 occurrence of a cold period around 1600 CE, with negative temperature anomalies persisting in Europe  
507 at decadal and multi-decadal scales (Ljungqvist et al., 2012; Luterbacher et al., 2016; Masson-Delmotte  
508 et al., 2013). Reconstructions of European summer temperature provided by Luterbacher et al. (2016)  
509 indicate that the coldest 11 and 51 year period since 755 CE in the area of Han-sur-Lesse cave occurred  
510 within the 17<sup>th</sup> century. These reconstructions showed a summer temperature decrease of 1 – 1.5°C  
511 around 1600-1650 CE. Although the 17<sup>th</sup> century has been recognized as the coldest of the past twelve





512 centuries, hydrological climate conditions appear close to the long-term mean (Ljungqvist et al., 2016),  
513 with no significant wetting or drying trend. However, to account for the differences between the 1960-  
514 2010 interval and the 17<sup>th</sup> century observed in this study, an increase in the amount winter  
515 precipitation is needed, suggesting that climatic conditions were wetter during that time. Such a  
516 hypothesis is also supported by the depleted  $\delta^{18}\text{O}$  values in P16, indicating an increase in winter  
517 precipitation.

## 518 **6. Conclusions**

519 This study of annual trace element and stable isotope ( $\delta^{13}\text{C}$  and  $\delta^{18}\text{O}$ ) variations over three different  
520 time intervals of the annually laminated Proserpine stalagmite from the Han-sur-Lesse Cave (Belgium)  
521 shows that seasonal changes in Mg, Sr and Ba during the recent period (1960-2010) suggest a strong  
522 effect of prior calcite precipitation, caused by lower water availability during summer. In the 17<sup>th</sup>  
523 century (1600 CE  $\pm$  30 and 1640 CE  $\pm$  30), however, Mg is in antiphase with Sr and Ba. This implies that  
524 another process overwrites the PCP dominated seasonal cycle in these trace elements. A varying  
525 degree of incongruent dolomite dissolution is the most plausible hypothesis, with more dissolution  
526 occurring during summer when water residence times in the epikarst are longer. The transfer function  
527 governing the trace elements, PCP or a varying degree of dolomite dissolution, depends on water-rock  
528 interaction. Stable isotope ratios ( $\delta^{13}\text{C}$  and  $\delta^{18}\text{O}$ ), soil derived trace element concentrations (Zn, Y and  
529 Pb) and speleothem morphology indicate that the multi-annual recharge of the epikarst was higher in  
530 the 17<sup>th</sup> century. The change in the response of Mg, Sr and Ba in the Proserpine speleothem to  
531 environmental changes was identified to be climate-driven and likely results from a recharge increase  
532 caused by a combination of lower summer temperatures and an increase in the amount of winter  
533 precipitation in the 17<sup>th</sup> century for the Han-sur-Lesse cave region. The effect of an increase in winter  
534 annual precipitation on the recharge is expected to be larger compared to a decrease in summer  
535 temperature. The data obtained in this study clearly shows a stronger seasonal cycle in cave hydrology  
536 during the 17<sup>th</sup> century.

537 This high-resolution, multi proxy study provides a good example of how seasonal proxy transfer  
538 functions of trace elements in speleothem calcite can change over time. Such an observation has  
539 implications for future speleothem-based paleoclimate reconstructions, since transfer functions for  
540 specific cave sites, determined by cave monitoring, are often assumed to remain constant when no  
541 drastic changes in the cave environment have occurred. As the change in trace element proxy transfer  
542 function observed in this study is climate-driven, this change by itself can serve as a valuable  
543 paleoclimate proxy.

544



545 **Author contributions**

546 Stef Vansteenberge and Sophie Verheyden designed the study. Stef Vansteenberge, Steven Goderis  
547 and Stijn Van Malderen carried out LA-ICP-MS measurements. Stef Vansteenberge, Matthias Sinnesael  
548 and Niels de Winter carried out stable isotope measurements. Stef Vansteenberge carried out the data  
549 processing and plotting with contributions from Steven Goderis, Niels de Winter and Matthias  
550 Sinnesael. Frank Vanhaecke and Philippe Claeys provided laboratory facilities and supported the  
551 measurements. Stef Vansteenberge, Niels de Winter and Matthias Sinnesael prepared the manuscript  
552 with contributions from all co-authors.

553

554 **Acknowledgements**

555 All authors thank the Domaine des Grottes de Han S.A. for allowing us to sample the stalagmites and  
556 carry out other fieldwork. Special thanks for M. Van Rampelbergh, whose PhD research formed the  
557 base of this study. S. Vansteenberge thanks J. Van Opendenbosch and A. Ndirembako for their help  
558 collecting the stable isotope data and D. Verstraeten for the lab assistance. This research was funded  
559 by the VUB Strategic Research Funding (S. Vansteenberge), FWO Flanders (M. Sinnesael and S.  
560 Goderis), IWT Flanders (N. J. de Winter), Research grant G017217N (S. J. M. Van Malderen and F.  
561 Vanhaecke) and the Hercules Foundation (upgrade of the VUB Stable Isotope Laboratory).

562



563 **Table 1**

|                           |                  |                  |                  |                 |                   |                   |                   |                                 |
|---------------------------|------------------|------------------|------------------|-----------------|-------------------|-------------------|-------------------|---------------------------------|
| Isotope                   | <sup>25</sup> Mg | <sup>27</sup> Al | <sup>29</sup> Si | <sup>31</sup> P | <sup>34</sup> S   | <sup>39</sup> K   | <sup>55</sup> Mn  | <sup>57</sup> Fe <sub>564</sub> |
| LOD (µg g <sup>-1</sup> ) | 4.0              | 9.0              | 100              | 1.0             | 7.0               | 7.0               | 0.08              | 4.0                             |
| Isotope                   | <sup>66</sup> Zn | <sup>85</sup> Rb | <sup>88</sup> Sr | <sup>89</sup> Y | <sup>137</sup> Ba | <sup>208</sup> Pb | <sup>232</sup> Th | <sup>238</sup> U <sub>565</sub> |
| LOD (µg g <sup>-1</sup> ) | 0.2              | 0.03             | 0.08             | 0.01            | 0.1               | 0.008             | 0.0005            | 0.0001 <sub>566</sub>           |

567 **Table 1:** Overview of limits of detection (LOD) of trace elements measured for this study using LA-ICP-

568 MS.



569 **Table 2**

| Proxy                   | P19   | P17  | P16  |
|-------------------------|---|--|--|
| Average Layer Thickness | Thin: 0.382 mm<br>Larger variations (RSD = 28.9%)   | Thick: 1.096 mm<br>Smaller variations (RSD = 6.3%)   | Thick: 1.135 mm<br>Smaller variations (RSD = 9.5%)   |
| $\delta^{18}\text{O}$   | Strong seasonality: tendency towards in phase correlation with $\delta^{13}\text{C}$<br><b>Partially T-controlled, but other processes as well</b>                        | Weak to no seasonality: unclear relation with $\delta^{13}\text{C}$  | Weak to no seasonality: unclear relation with $\delta^{13}\text{C}$  |
| $\delta^{13}\text{C}$   | Clear $\delta^{13}\text{C}$ cycle:<br>Low $\delta^{13}\text{C}$ mostly in DCL but not always<br><b><math>\delta^{13}\text{C}</math> driven by seasonal changes in PCP</b> | Clear $\delta^{13}\text{C}$ cycle:<br>Low $\delta^{13}\text{C}$ always in DCL<br><b><math>\delta^{13}\text{C}</math> driven by seasonal changes in PCP</b> | Clear $\delta^{13}\text{C}$ cycle:<br>Low $\delta^{13}\text{C}$ always in DCL<br><b><math>\delta^{13}\text{C}</math> driven by seasonal changes in PCP</b> |
| Mg and Sr - Ba          | Good in phase correlation<br><b>Mg, Sr and Ba driven by seasonal changes in PCP</b>   | Phase relation not clear<br><b>Transition period between P16 and P19 hydrological regimes</b>  | Anti-phase correlation between Mg and Sr, Ba<br><b>Seasonally occurring IDD dominates over PCP</b>   |
| Zn, Y and Pb            | Weak seasonality in Zn and Y,<br>Strong seasonality in Pb<br><b>Decreased flushing, anthropogenic Pb enrichment</b>   | Weak seasonality in Zn, Y and Pb<br><b>Decreased flushing</b>  | Very strong seasonality in Zn and Y,<br>weak seasonality in Pb<br><b>Enhanced flushing</b>   |
| U                       | Strong seasonality, antiphase with Mg, Sr and Ba<br><b>No PCP control, scavenging</b>   | Weak seasonality antiphase with Sr and Ba<br><b>scavenging</b>   | No seasonality   |
| Remarks                 | Link with trace elements and layering is challenging  | Link with trace elements and layering is challenging   | Link with trace elements and layering is challenging   |

570  
 571 **Table 2: Schematic overview providing the observed changes and interpretation for the different proxies of P19, P17 and P16. PCP = prior**  
 572 **calcite precipitation, IDD = incongruent dissolution of dolomite, DCL = dark compact layers, WPL = white porous layers**

570

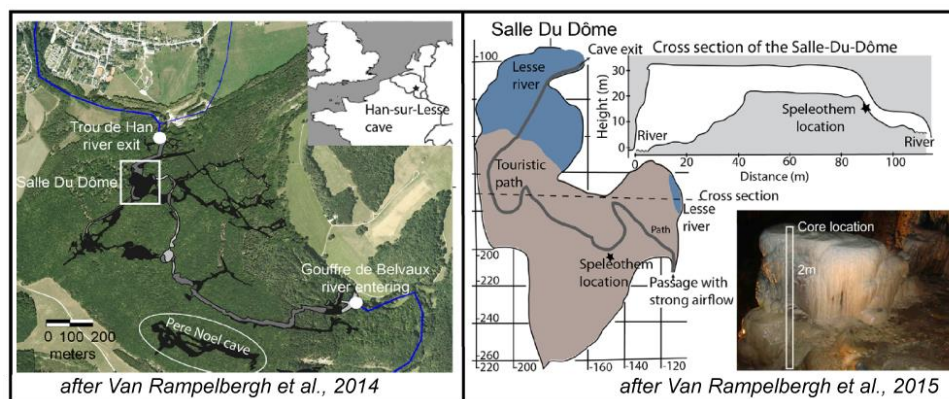
571

572

573



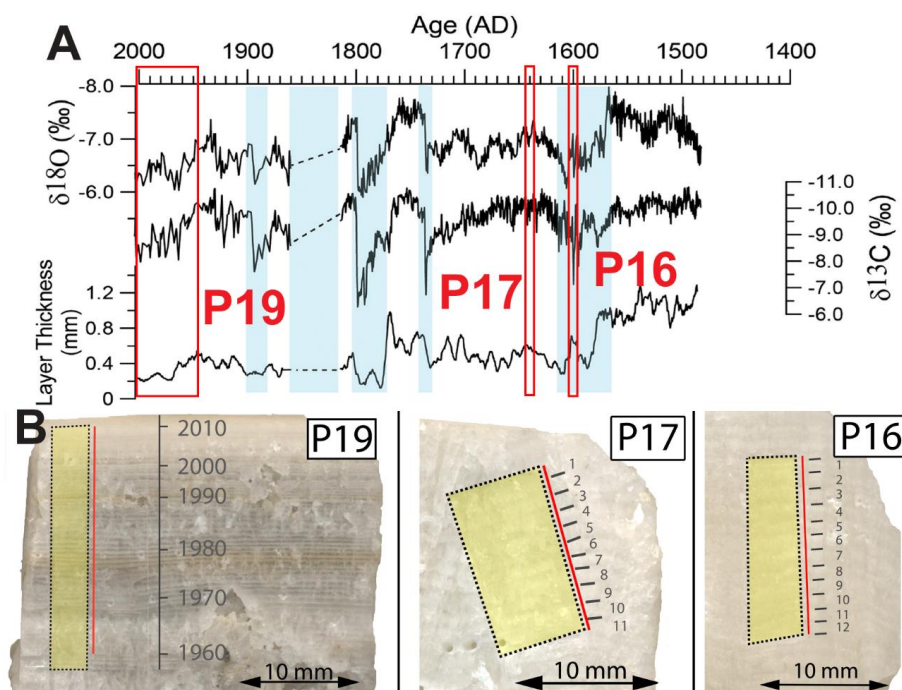
574 **FIGURES**



575

576 **Figure 1:** (left) Location of the Han-sur-Lesse Cave system (N50.114251, E5.203342) with the entrance  
577 and exit of the Lesse River, the Salle-du-dome and the Père-Noël Cave. North is upwards (right) Map  
578 showing the location of the Proserpine stalagmite within the Salle-du-Dome. The insert shows the  
579 position of the core retrieved from the speleothem. Images adapted from Van Rampelbergh et al.  
580 (2014, 2015).

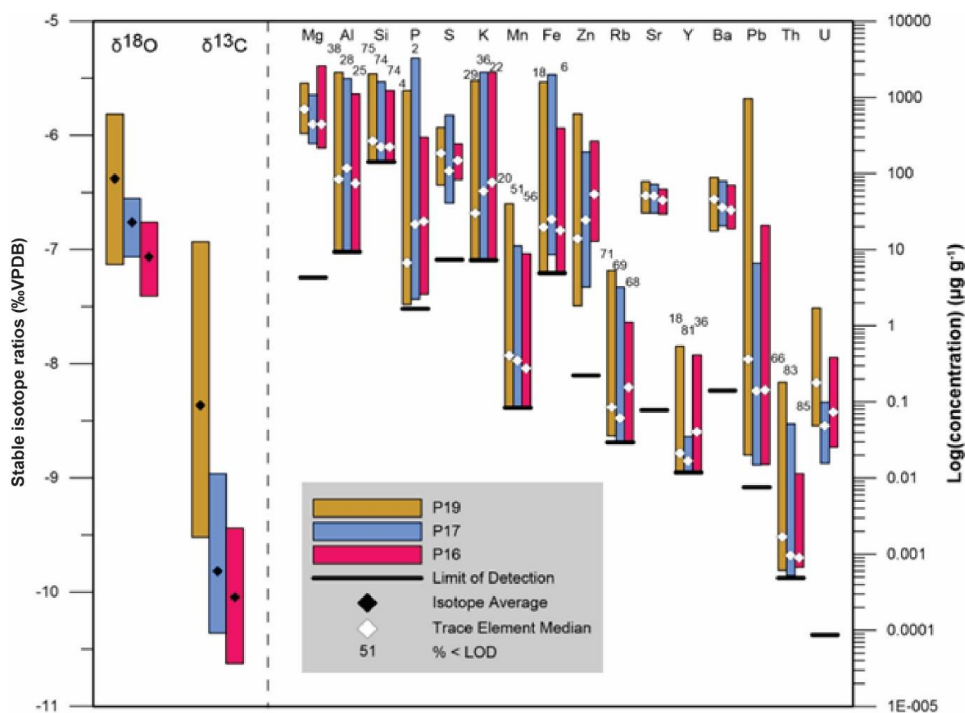
581



582

583 **Figure 2:** A. Overview of long (~500 yr) record of stable isotope ratios and annual layer thickness  
584 through the Proserpine speleothem measured by Van Rampelbergh et al. (2015). Red boxes indicate  
585 the locations of high-resolution transects discussed in this study. B. The three studied growth periods  
586 P19 (1960-2010 CE), P17 (1633-1644 ± 30 CE) and P16 (1593-1605 ± 30 CE). The yellow rectangles mark  
587 the sections that were drilled/sampled for  $\delta^{13}\text{C}$  and  $\delta^{18}\text{O}$  analysis, the red lines represent the LA-ICP-  
588 MS transects. Numbers in grey indicate the observed layer couplets.

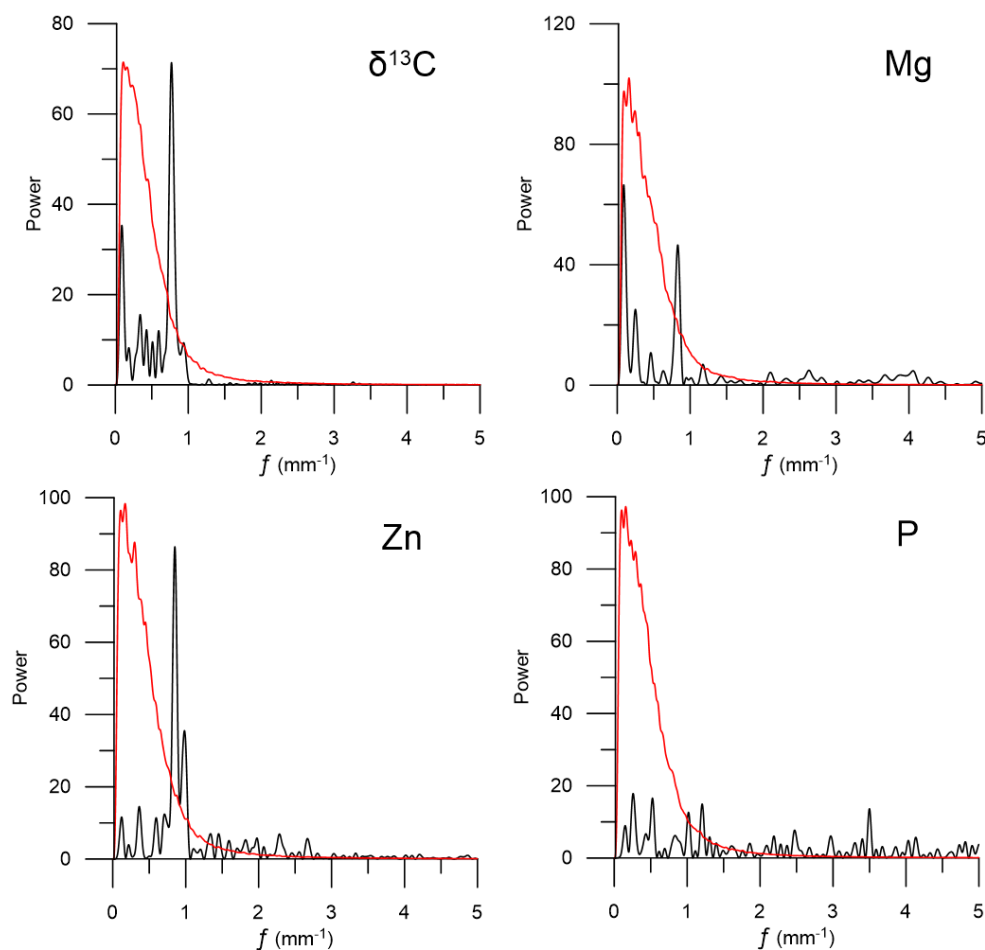
589



590

591 **Figure 3:** Ranges of the stable isotope (left) and trace element data (right). For the stable isotope  
592 ratios, the data mark the average (black diamonds) and the standard deviation ( $1\sigma$ ) of the  
593 distribution. For the trace element concentrations, the boxes represent the minimum and maximum  
594 values and the white diamonds mark the median. Numbers on top of the bars represent the  
595 percentage of the data that is below the calculated detection limit.

596

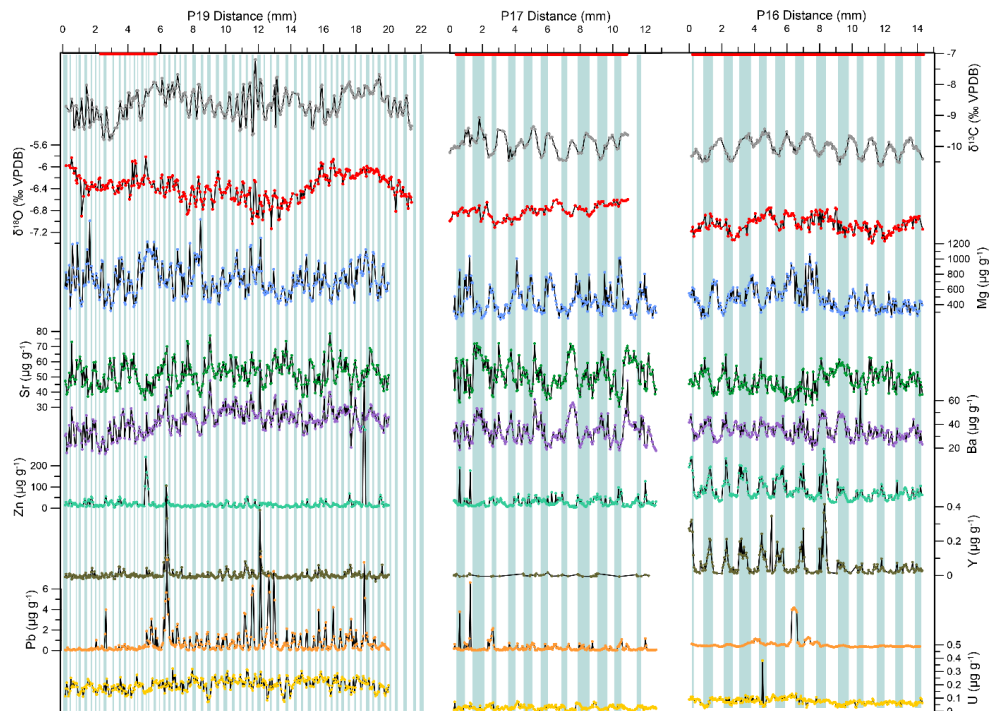


597

598 **Figure 4:** Periodograms (FFT) of  $\delta^{13}\text{C}$ , Mg, Zn and P measured in P16 to illustrate how the quality of a  
599 proxy to record the seasonal cycle can be studied. The red line represents the 95% confidence level.  
600  $\delta^{13}\text{C}$  is taken as a reference. The periodograms include two examples of proxies with a distinct peak in  
601 the seasonal frequency band of  $0.8 \text{ mm}^{-1}$  (Mg and Zn) and one proxy with no peak in the seasonal  
602 frequency band. Periodograms for all periods are provided in the supplementary material.

603

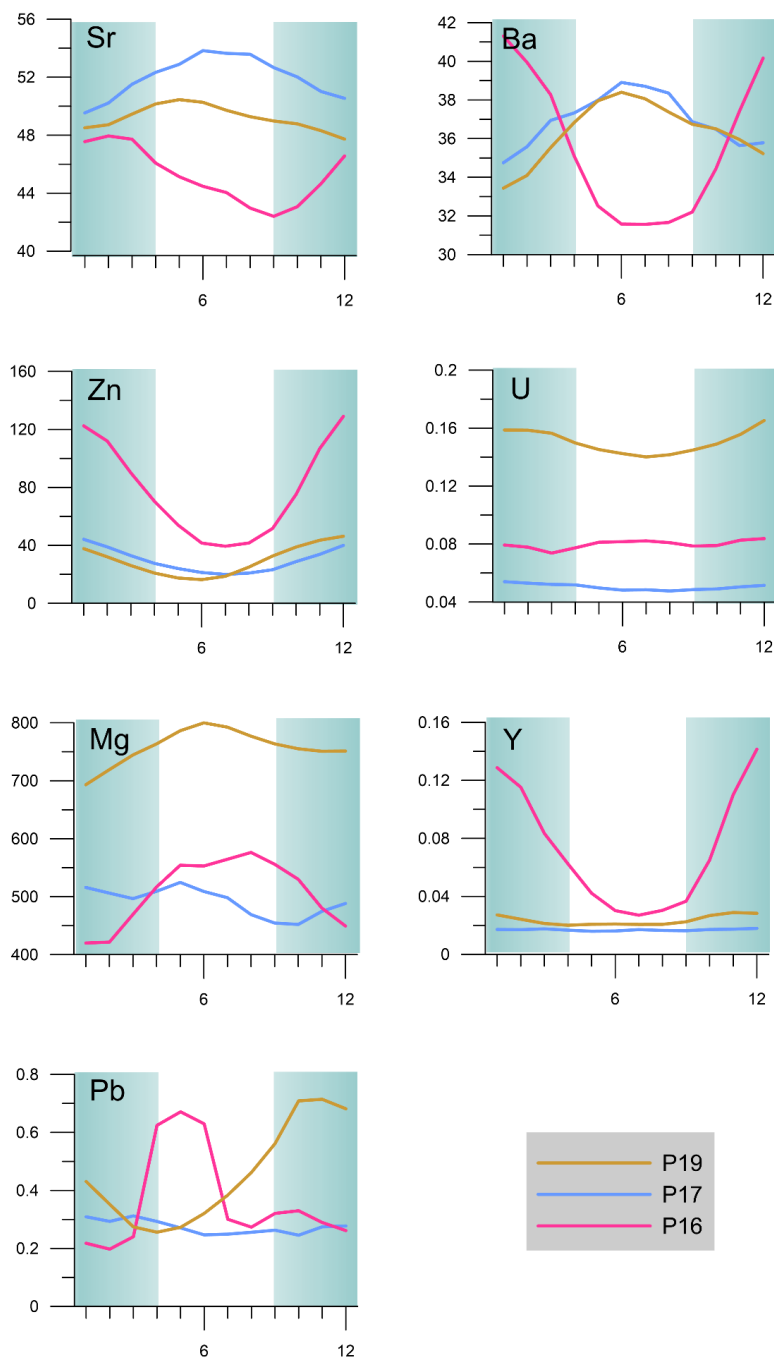




604

605 **Figure 5:** Stable isotope ratios and trace element variations plotted against distance for P19, P17 and  
606 P16. Blue bars mark the DCC laminae. The left side represents the youngest layers. All stable isotope  
607 ratios are expressed as ‰ VPDB, while trace element concentrations are reported in ppm. Red bars  
608 indicate years used for annual stack (Fig. 5 and 6).

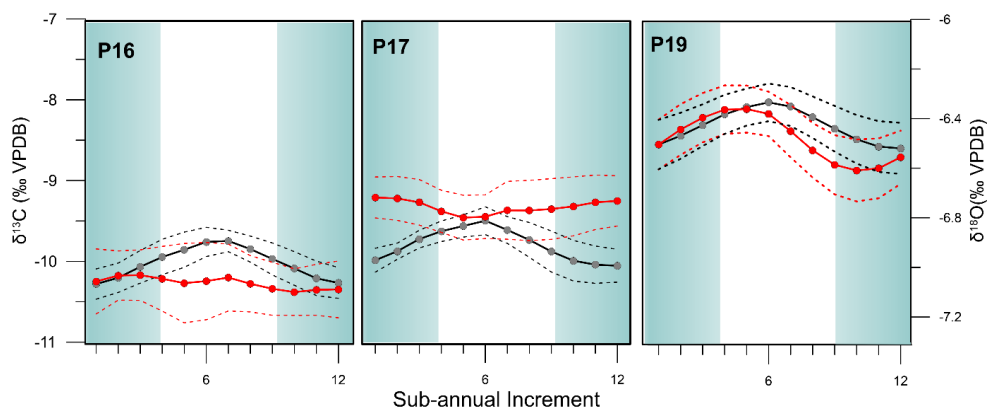
609



610

611 **Figure 6:** Annual stacks of the trace element proxies. Y-axis: concentrations ( $\mu\text{g g}^{-1}$ ); x-axis: sub-annual  
612 increment. For the years used, see Fig. 5.

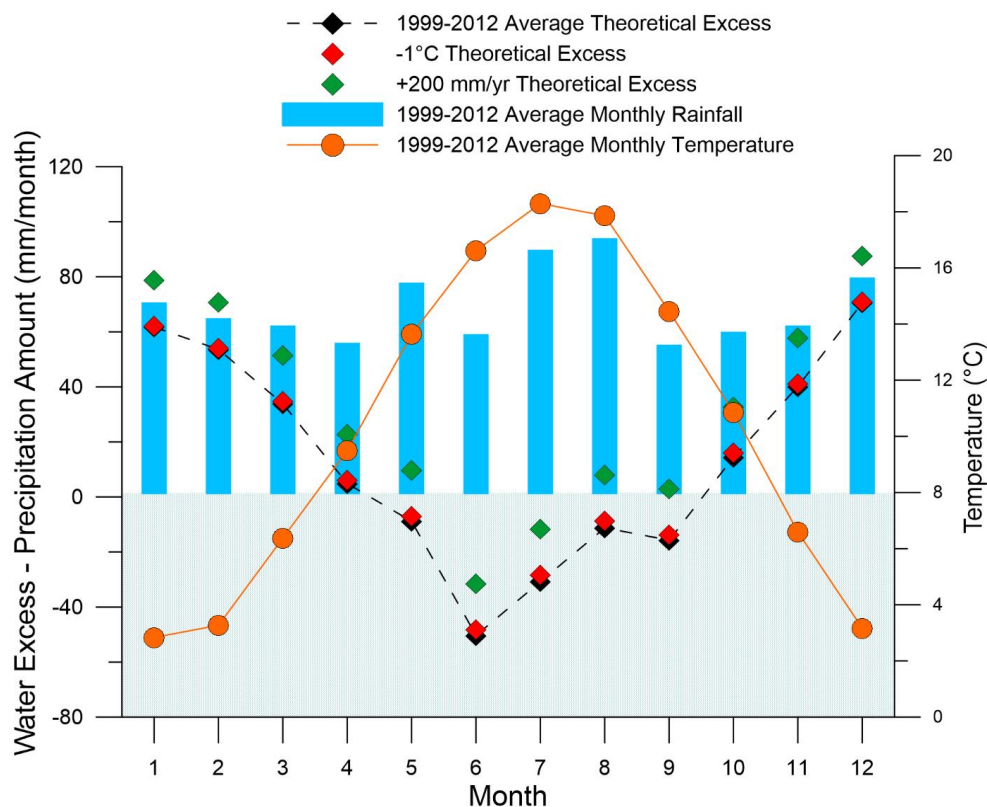
613



614

615 **Figure 7:** Annual stacks of  $\delta^{13}\text{C}$  (black) and  $\delta^{18}\text{O}$  (red). Dashed lines mark the  $2\sigma$  uncertainty. The x-axis  
616 represents one year. For the years used, see Fig. 5.

617



618

619 **Figure 8:** Chart showing the calculated theoretical amount of water excess calculated with the  
 620 Thornthwaite equation (Thornthwaite and Mather, 1957), based on temperature and precipitation  
 621 data near Han-sur-Lesse cave from 1999 to 2012 (Royal Meteorological Institute, KMI). X-axis  
 622 represents the months from January to December.



623

## 624 References

- 625 Allan, M., Fagel, N., Van Rempelbergh, M., Baldini, J., Riotte, J., Cheng, H., Edwards, R.L., Gillikin, D., Quinif, Y., Verheyden, S.: Lead  
626 concentrations and isotope ratios in speleothems as proxies for atmospheric metal pollution since the industrial revolution. *Chem. Geol.*  
627 401, 140-150, 2015.
- 628 Baker, A., Genty, D., Dreybrodt, W., Barnes, W.L., Mockler, N.J., Grapes, J.: Testing theoretically predicted stalagmite growth rate with Recent  
629 annually laminated samples: Implications for past stalagmite deposition. *Geochim. Cosmochim. Acta* 62, 393-404, 1998.
- 630 Baker, A., Smith, C.L., Jex, C., Fairchild, I.J., Genty, D., Fuller, L.: Annually Laminated Speleothems: a Review. *Int. J. Speleol.* 37, 193-206, 2008.
- 631 Baker, A., Wilson, R., Fairchild, I.J., Franke, J., Spötl, C., Matthey, D., Trouet, V., Fuller, L.: High resolution  $\delta^{18}O$  and  $\delta^{13}C$  records from an  
632 annually laminated Scottish stalagmite and relationship with last millennium climate. *Glob. Planet. Change* 79, 303-311, 2011.
- 633 Baldini, J.U.L., McDermott, F., Fairchild, I.J.: Structure of the 8200-year cold event revealed by a speleothem trace element record. *Science*  
634 296, 2203-2206, 2002.
- 635 Bauer, E., Claussen, M., Brovkin, V., Huenerbein, A.: Assessing climate forcings of the Earth system for the past millennium. *Geophys. Res.*  
636 *Lett.* 30, 1276-1282, 2003.
- 637 Bice, D., Montanari, A., Vucetic, V., Vucetic, M.: The influence of regional and global climatic oscillations on Croatian climate. *Int. J. Climatol.*  
638 32, 1537-1557, 2012.
- 639 Black, P.E.: Revisiting the Thornthwaite and Mather water balance. *J. Am. Water Resour. Assoc.* 43, 1604-1605, 2007.
- 640 Borsato, A., Frisia, S., Fairchild, I.J., Somogyi, A., Susini, J.: Trace element distribution in annual stalagmite laminae mapped by micrometer-  
641 resolution X-ray fluorescence: Implications for incorporation of environmentally significant species. *Geochim. Cosmochim. Acta* 71, 1494-  
642 1512, 2007.
- 643 Bourdin, C., Douville, E., Genty, D. Alkaline-earth metal and rare-earth element incorporation control by ionic radius and growth rate on a  
644 stalagmite from the Chauvet Cave, Southeastern France. *Chem. Geol.* 290, 1-11, 2011.
- 645 Crowley, T.J.: Causes of Climate Change Over the Past 1000 Years. *Science* 289, 270, 2000.
- 646 Cui, Y.F., Wang, Y.J., Cheng, H., Zhao, K., Kong, X.G.: Isotopic and lithologic variations of one precisely-dated stalagmite across the  
647 Medieval/LIA period from Heilong Cave, central China. *Clim. Past* 8, 1541-1550, 2012.
- 648 D'Arrigo, R., Wilson, R., Jacoby, G.: On the long-term context for late twentieth century warming. *J. Geophys. Res. Atmos.* 111, 12, 2006.
- 649 Day, C.C., Henderson, G.M.: Controls on trace-element partitioning in cave-analogue calcite. *Geochim. Cosmochim. Acta* 120, 612-627, 2013.
- 650 de Winter, N.J., Goderis, S., Dehairs, F., Jagt, J.W., Fraaije, R.H., Van Malderen, S.J., Vanhaecke, F., Claeys, P.: Tropical seasonality in the late  
651 Campanian (late Cretaceous): Comparison between multiproxy records from three bivalve taxa from Oman. *Palaeogeography,*  
652 *Palaeoclimatology, Palaeoecology* 485, 740-760, 2017.
- 653 de Winter, N.J., Vellekoop, J., Vorrsselmans, R., Golreihan, A., Soete, J., Petersen, S.V., Meyer, K.W., Casadio, S., Speijer, R.P., Claeys, P.: An  
654 assessment of latest Cretaceous Pycnodonte vesicularis (Lamarck, 1806) shells as records for palaeoseasonality: a multi-proxy  
655 investigation. *Climate of the Past* 14, 725-749, 2018.
- 656 Dobrovolny, P., Moberg, A., Brazdil, R., Pfister, C., Glaser, R., Wilson, R., van Engelen, A., Limanowka, D., Kiss, A., Halickova, M., Mackova, J.,  
657 Riemann, D., Luterbacher, J., Bohm, R.: Monthly, seasonal and annual temperature reconstructions for Central Europe derived from  
658 documentary evidence and instrumental records since AD 1500. *Clim. Change* 101, 69-107, 2010.
- 659 Fairchild, I.J., Baker, A., Borsato, A., Frisia, S., Hinton, R.W., McDermott, F., Tooth, A.F.: Annual to sub-annual resolution of multiple trace-  
660 element trends in speleothems. *J. Geol. Soc. London* 158, 831-841, 2001.
- 661 Fairchild, I.J., Borsato, A., Tooth, A.F., Frisia, S., Hawkesworth, C.J., Huang, Y.M., McDermott, F., Spiro, B.: Controls on trace element (Sr-Mg)  
662 compositions of carbonate cave waters: implications for speleothem climatic records. *Chem. Geol.* 166, 255-269, 2000.
- 663 Fairchild, I.J., Spötl, C., Frisia, S., Borsato, A., Susini, J., Wynn, P.M., Cauzid, J., Eimf.: Petrology and geochemistry of annually laminated  
664 stalagmites from an Alpine cave (Obir, Austria): seasonal cave physiology. *Geol. Soc. London, Special Publications* 336, 295-321, 2010.
- 665 Fairchild, I.J., Treble, P.C.: Trace elements in speleothems as recorders of environmental change. *Quat. Sci. Rev.* 28, 449-468, 2009.
- 666 Friedman, I., O'Neil, J., Cebula, G.: Two New Carbonate Stable-Isotope Standards. *Geostandards Newsletter* 6, 11-12, 1982.
- 667 Frisia, S., Borsato, A., Drysdale, R.N., Paul, B., Greig, A., Cotte, M.: A re-evaluation of the palaeoclimatic significance of phosphorus variability  
668 in speleothems revealed by high-resolution synchrotron micro XRF mapping. *Clim. Past* 8, 2039-2051, 2012.



- 669 Gascoyne, M.: Trace-element partition-coefficients in the calcite water-system and their paleoclimatic significance in cave studies. *J. Hydrol.*  
670 61, 213-222, 1983.
- 671 Genty, D., Baker, A., Massault, M., Proctor, C., Gilmour, M., Pons-Branchu, E., Hamelin, B.: Dead carbon in stalagmites: Carbonate bedrock  
672 paleodissolution vs. ageing of soil organic matter. Implications for C-13 variations in speleothems. *Geochim. Cosmochim. Acta* 65, 3443-  
673 3457, 2001.
- 674 Genty, D., Blamart, D., Ouahdi, R., Gilmour, M., Baker, A., Jouzel, J., Van-Exter, S.: Precise dating of Dansgaard-Oeschger climate oscillations  
675 in western Europe from stalagmite data. *Nature* 421, 833-837, 2003.
- 676 Genty, D., Deflandre, G.: Drip flow variations under a stalactite of the Pere Noel cave (Belgium). Evidence of seasonal variations and air  
677 pressure constraints. *J. Hydrol.* 211, 208-232, 1998.
- 678 Genty, D., Quinif, Y.: Annually laminated sequences in the internal structure of some Belgian stalagmites - Importance for paleoclimatology.  
679 *J. Sediment. Res.* 66, 275-288, 1996.
- 680 Gimeno, L., Drumond, A., Nieto, R., Trigo, R.M., Stohl, A.: On the origin of continental precipitation. *Geophys. Res. Lett.* 37, L13804, 2010.
- 681 Hartland, A., Fairchild, I.J., Lead, J.R., Borsato, A., Baker, A., Frisia, S., Baalousha, M.: From soil to cave: Transport of trace metals by natural  
682 organic matter in karst dripwaters. *Chem. Geol.* 304, 68-82, 2012.
- 683 Huang, Y.M., Fairchild, I.J.: Partitioning of Sr<sup>2+</sup> and Mg<sup>2+</sup> into calcite under karst-analogue experimental conditions. *Geochim. Cosmochim.*  
684 *Acta* 65, 47-62, 2001.
- 685 Jamieson, R. A., Baldini, J. U., Frappier, A. B., & Müller, W.: Volcanic ash fall events identified using principal component analysis of a high-  
686 resolution speleothem trace element dataset. *Earth and Planetary Science Letters*, 426, 36-45, 2015.
- 687 Jamieson, R.A., Baldini, J.U.L., Brett, M.J., Taylor, J., Ridley, H.E., Ottley, C.J., Prufer, K.M., Wassenburg, J.A., Scholz, D., Breitenbach, S.F.M.:  
688 Intra- and inter-annual uranium concentration variability in a Belizean stalagmite controlled by prior aragonite precipitation: A new tool  
689 for reconstructing hydro-climate using aragonitic speleothems. *Geochim. Cosmochim. Acta* 190, 332-346, 2016.
- 690 Johnson, K.R., Hu, C.Y., Belshaw, N.S., Henderson, G.M. Seasonal trace-element and stable-isotope variations in a Chinese speleothem: The  
691 potential for high-resolution paleomonsoon reconstruction. *Earth Planet. Sci. Lett.* 244, 394-407, 2006.
- 692 Kottek, M., Grieser, J., Beck, C., Rudolf, B., Rubel, F. World Map of the Köppen-Geiger climate classification updated. *Meteorol. Zeit.* 15, 259-  
693 263, 2006.
- 694 Lachniet, M.S.: Climatic and environmental controls on speleothem oxygen-isotope values. *Quat. Sci. Rev.* 28, 412-432, 2009.
- 695 Ljungqvist, F.C., Krusic, P.J., Brattstrom, G., Sundqvist, H.S.: Northern Hemisphere temperature patterns in the last 12 centuries. *Clim. Past* 8,  
696 227-249, 2012.
- 697 Ljungqvist, F.C., Krusic, P.J., Sundqvist, H.S., Zorita, E., Brattström, G., Frank, D.: Northern Hemisphere hydroclimate variability over the past  
698 twelve centuries. *Nature* 532, 94-98, 2016.
- 699 Lohmann, K.C.: Geochemical Patterns of Meteoric Diagenetic Systems and Their Application to Studies of Paleokarst, in: N.P. James, P.W.  
700 Choquette (Eds.), *Paleokarst*. Springer New York, New York, pp. 58-80, 1988.
- 701 Luterbacher, J., Werner, J.P., Smerdon, J.E., Fernandez-Donado, L., Gonzalez-Rouco, F.J., Barriopedro, D., Ljungqvist, F.C., Buntgen, U., Zorita,  
702 E., Wagner, S., Esper, J., McCarroll, D., Toreti, A., Frank, D., Jungclauss, J.H., Barriendos, M., Bertolin, C., Bothe, O., Brazdil, R., Camuffo,  
703 D., Dobrovolny, P., Gagen, M., Garica-Bustamante, E., Ge, Q., Gomez-Navarro, J.J., Guiot, J., Hao, Z., Hegerl, G.C., Holmgren, K., Klimentko,  
704 V.V., Martin-Chivelet, J., Pfister, C., Roberts, N., Schindler, A., Schurer, A., Solomina, O., von Gunten, L., Wahl, E., Wanner, H., Wetter, O.,  
705 Xoplaki, E., Yuan, N., Zanchettin, D., Zhang, H., Zerefos, C.: European summer temperatures since Roman times. *Environ. Res. Lett.* 11,  
706 12, 2016.
- 707 Masson-Delmotte, V., Schulz, M., Abe-Ouchi, A., Beer, J., Ganopolski, A., González Rouco, J.F., Jansen, E., Lambeck, K., Luterbacher, J., Naish,  
708 T., Osborn, T., Otto-Bliesner, B., Quinn, T., Ramesh, R., Rojas, M., Shao, X., Timmermann, A.: Information from Paleoclimate Archives, in:  
709 Stocker, T.F., Qin, D., Plattner, G.-K., Tignor, M., Allen, S.K., Boschung, J., Nauels, A., Xia, Y., Bex, V., Midgley, P.M. (Eds.), *Climate Change*  
710 2013: The Physical Science Basis. Contribution of Working Group I to the Fifth Assessment Report of the Intergovernmental Panel on  
711 Climate Change. Cambridge University Press, Cambridge, United Kingdom and New York, NY, USA, 2013.
- 712 Meyers, S.R.: Astrochron: An R Package for Astrochronology. <https://cran.r-project.org/package=astrochron> (accessed March 2017), 2014.
- 713 Muller, R.A., MacDonald, G.J.: Ice Ages and Astronomical Causes: Data, Spectral Analysis and Mechanisms. Springer, London, U.K., pp. 318,  
714 2000.
- 715 Oster, J.L., Montanez, I.P., Mertz-Kraus, R., Sharp, W.D., Stock, G.M., Spero, H.J., Tinsley, J., Zachos, J.C.: Millennial-scale variations in western  
716 Sierra Nevada precipitation during the last glacial cycle MIS 4/3 transition. *Quat. Res.* 82, 236-248, 2014.



- 717 Ahmed, M., Anchukaitis, K.J., Asrat, A., Borgaonkar, H.P., Braida, M., Buckley, B.M., Büntgen, U., Chase, B.M., Christie, D.A., Cook, E.R.,  
718 Curran, M.A.J., Diaz, H.F., Esper, J., Fan, Z.X., Gaire, N.P., Ge, Q., Gergis, J., Rouco, J.F.G., Goosse, H., Grab, S.W., Graham, N., Graham,  
719 R., Grosjean, M., Hanhijärvi, S.T., Kaufman, D.S., Kiefer, T., Kimura, K., Korhola, A.A., Krusic, P.J., Lara, A., Lézine, A.M., Ljungqvist, F.C.,  
720 Lorrey, A.M., Luterbacher, J., Masson-Delmotte, V., McCarroll, D., McConnell, J.R., McKay, N.P., Morales, M.S., Moy, A.D., Mulvaney,  
721 R., Mundo, I.A., Nakatsuka, T., Nash, D.J., Neukom, R., Nicholson, S.E., Oerter, H., Palmer, J.G., Phipps, S.J., Prieto, M.R., Rivera, A.,  
722 Sano, M., Severi, M., Shanahan, T.M., Shao, X., Shi, F., Sigl, M., Smerdon, J.E., Solomina, O.N., Steig, E.J., Stenni, B., Thamban, M.,  
723 Trouet, V., Turney, C.S.M., Umer, M., van Ommen, T., Verschuren, D., Viau, A.E., Villalba, R., Vinther, B.M., von Gunten, L., Wagner, S.,  
724 Wahl, E.R., Wanner, H., Werner, J.P., White, J.W.C., Yasue, K., Zorita E.: Continental-scale temperature variability during the past two  
725 millennia. *Nature Geosci.* 6, 339-346, 2013.
- 726 Pas, D., Da Silva, A.C., Devleeschouwer, X., De Vleeschouwer, D., Cornet, P., Labaye, C., Boulvain, F.: Insights into a million-year-scale  
727 Rhenohercynian carbonate platform evolution through a multi-disciplinary approach: example of a Givetian carbonate record from  
728 Belgium. *Geol. Mag.* 1-33, 2016.
- 729 Pingitore, N.E., Eastman, M.P.: The coprecipitation of Sr<sup>2+</sup> with calcite at 25 degrees C and 1 Atm. *Geochim. Cosmochim. Acta* 50, 2195-2203,  
730 1986.
- 731 Regattieri, E., Zanchetta, G., Drysdale, R. N., Isola, I., Woodhead, J. D., Hellstrom, J. C., Giaccio, B., Greig, A., Baneschi, I., Dotsika, E.:  
732 Environmental variability between the penultimate deglaciation and the mid Eemian: Insights from Tana che Urla (central Italy)  
733 speleothem trace element record. *Quaternary Science Reviews*, 152, 80-92, 2016.
- 734 Ridley, H.E., Baldini, J.U.L., Pruffer, K.M., Walczak, I.W., Breitenbach, S.F.M.: High-resolution monitoring of Yok Balum Cave, Belize: an  
735 investigation of seasonal ventilation regimes and the atmospheric and drip-flow response to a local earthquake. *J. Cave Karst Stud.* 77,  
736 183-199, 2015.
- 737 Rimstidt, J.D., Balog, A., Webb, J.: Distribution of trace elements between carbonate minerals and aqueous solutions. *Geochimica et*  
738 *Cosmochimica Acta* 62, 1851-1863. Roberts, M.S., Smart, P.L., Baker, A., 1998. Annual trace element variations in a Holocene  
739 speleothem. *Earth Planet. Sci. Lett.* 154, 237-246, 1998.
- 740 Rozanski, K., Araguas-Araguas, L., Gonfiantini, R.: Relation between long-term trends of O-18 isotope composition of precipitation and climate.  
741 *Science* 258, 981-985, 1992.
- 742 Smith, C.L., Fairchild, I.J., Spotl, C., Frisia, S., Borsato, A., Moreton, S.G., Wynn, P.M.: Chronology building using objective identification of  
743 annual signals in trace element profiles of stalagmites. *Quat. Geochronol.* 4, 11-21, 2009.
- 744 Thornthwaite, C.W., Mather, J.R.: Instructions and Tables for the Computing Potential Evapotranspiration and the Water Balance.  
745 *Publications in Climatology* 10, 311, 1957.
- 746 Treble, P., Shelley, J.M.G., Chappell, J.: Comparison of high resolution sub-annual records of trace elements in a modern (1911-1992)  
747 speleothem with instrumental climate data from southwest Australia. *Earth Planet. Sci. Lett.* 216, 141-153, 2003.
- 748 Van Rampelbergh, M., Verheyden, S., Allan, M., Quinif, Y., Keppens, E., Claeys, P.: Seasonal variations recorded in cave monitoring results  
749 and a 10 year monthly resolved speleothem  $\delta^{18}\text{O}$  and  $\delta^{13}\text{C}$  record from the Han-sur-Lesse cave, Belgium. *Climate of the Past*  
750 *Discussions* 10, 1821-1856, 2014.
- 751 Van Rampelbergh, M., Verheyden, S., Allan, M., Quinif, Y., Cheng, H., Edwards, L.R., Keppens, E., Claeys, P.: A 500-year seasonally resolved  
752  $\delta^{18}\text{O}$  and  $\delta^{13}\text{C}$ , layer thickness and calcite aspect record from a speleothem deposited in the Han-sur-Lesse cave, Belgium. *Climate of*  
753 *the Past* 11, 789-802, 2015.
- 754 Verheyden, S., Baele, J.M., Keppens, E., Genty, D., Cattani, O., Hai, C., Edwards, L., Hucai, Z., Van Strijdonck, M., Quinif, Y.: The proserpine  
755 stalagmite (Han-sur-Lesse cave, Belgium): Preliminary environmental interpretation of the last 1000 years as recorded in a layered  
756 speleothem. *Geol. Belg.* 9, 245-256, 2006.
- 757 Verheyden, S., Genty, D., Deflandre, G., Quinif, Y., Keppens, E.: Monitoring climatological, hydrological and geochemical parameters in the  
758 Pere Noel cave (Belgium): implication for the interpretation of speleothem isotopic and geochemical time-series. *Int. J. Speleol.* 37, 221-  
759 234, 2008.
- 760 Wang, Y.J., Cheng, H., Edwards, R.L., An, Z.S., Wu, J.Y., Shen, C.C., Dorale, J.A.: A High-Resolution Absolute-Dated Late Pleistocene Monsoon  
761 Record from Hulu Cave, China. *Science* 294, 2345-2348, 2001.
- 762 Warken, S. F., Fohlmeister, J., Schröder-Ritzrau, A., Constantin, S., Spötl, C., Gerdes, A., Esper, J., Frank, N., Arps, J., Terente, M., Riechelmann,  
763 D.F.C., Mangini, A., Riechelmann, D. F.: Reconstruction of late Holocene autumn/winter precipitation variability in SW Romania from a  
764 high-resolution speleothem trace element record. *Earth and Planetary Science Letters*, 499, 122-133, 2018.



- 765 Wynn, P.M., Fairchild, I.J., Spotl, C., Hartland, A., Matthey, D., Fayard, B., Cotte, M.: Synchrotron X-ray distinction of seasonal hydrological and  
766 temperature patterns in speleothem carbonate. *Environ. Chem.* **11**, 28-36, 2014.
- 767 Zennaro, P., Kehrwald, N., McConnell, J.R., Schupbach, S., Maselli, O.J., Marlon, J., Vallelonga, P., Leuenberger, D., Zangrando, R., Spolaor, A.,  
768 Borrotti, M., Barbaro, E., Gambaro, A., Barbante, C.: Fire in ice: two millennia of boreal forest fire history from the Greenland NEEM ice  
769 core. *Clim. Past* **10**, 1905-1924, 2014.